

Wilson mass dependence of the overlap topological charge density

Peter J. Moran^{a,c}, Derek B. Leinweber^a, J. B. Zhang^{a,b}

^a*Special Research Center for the Subatomic Structure of Matter (CSSM) and
Department of Physics, University of Adelaide 5005, Australia*

^b*ZIMP and Department of Physics, Zhejiang University, Hangzhou, 310027,
People's Republic of China*

^c*CSIRO Mathematics, Informatics and Statistics,
Private Bag 33, Clayton South, VIC 3169, Australia*

Abstract

The dependence of the overlap Dirac operator on the Wilson-mass regulator parameter is studied through calculations of the overlap topological charge densities at a variety of Wilson-mass values, using a Lüscher-Weisz gauge action. In this formulation, the Wilson-mass is used in the negative mass region and acts as a regulator governing the scale at which the Dirac operator is sensitive to topological aspects of the gauge field. We observe a clear dependence on the value of the Wilson-mass and demonstrate how these values can be calibrated against a finite number of stout-link smearing sweeps. The overlap topological charge density is also computed using a pre-smear gauge field for the input kernel. We show how applying the overlap operator leads to further filtering of the gauge field. The results suggest that the freedom typically associated with smearing algorithms, through the variable number of sweeps, also exists in the overlap operator, through the variable Wilson-mass parameter.

Keywords: overlap, fat-link fermions, stout-link, smearing, topological charge density, topology, vacuum structure

PACS: 12.38.Gc, 11.15.Ha, 12.38.Aw, 14.65.-q

1. Introduction

The topological structure of the QCD vacuum has been the subject of many lattice investigations over the years. Local patterns in topological charge fluctuations represent a significant aspect of this structure. Moreover, important physical phenomena such as a large η' mass, θ dependence, and possibly spontaneous chiral symmetry breaking are directly related to vacuum fluctuations of the topological charge. By the axial anomaly, matrix elements or correlation functions involving the topological charge density operator $q(x)$ can be related to relevant quantities of hadronic phenomenology.

Lattice QCD enables non-perturbative studies of the strong interaction from first principles, and should prove useful for studying the important topological structure of the vacuum. Unfortunately, obtaining a lattice discretization for studying topology is not completely straightforward,

Email addresses: peter.moran@alumni.adelaide.edu.au (Peter J. Moran),
derek.leinweber@adelaide.edu.au (Derek B. Leinweber), jbzhang08@zju.edu.cn (J. B. Zhang)

Preprint submitted to Elsevier

September 21, 2018

e.g. naively discretizing the topological charge density generally leads to non-integer values for the topological charge. Physical hadronic interactions also observe an approximate chiral symmetry that is described by the theory of QCD, where in the massless limit, an exact chiral symmetry is realized. Unfortunately, naive transcriptions of the continuum theory explicitly break chiral symmetry at finite lattice spacing a .

The Wilson Dirac operator [1],

$$D_W = \sum_{\mu} \left(\gamma_{\mu} \nabla_{\mu} - \frac{1}{2} r a \Delta_{\mu} + m \right), \quad (1)$$

contains the irrelevant Wilson term, $r \Delta_{\mu}/2$, that explicitly breaks chiral symmetry at $\mathcal{O}(a)$ in order to remove fermion doublers. This lattice discretisation is often improved through the introduction of a clover term [2], however issues with chiral symmetry breaking still exist.

One technique that has recently been used to successfully reproduce the light hadron spectrum [3], is to filter the gauge links prior to applying the Dirac operator. These types of fermion actions are typically referred to as UV-filtered or fat-link actions. The term “fat-link” comes from the smeared, *i.e.* fat, links that are used to construct the Dirac operator. One can smear either all links [4, 5, 6, 7, 8], only the irrelevant terms [9, 10, 11, 12], or even just the relevant terms [13]. Incorporating at least some amount of UV-filtering has been shown to reduce the effects of chiral symmetry breaking [4, 7, 14, 11, 12, 15]. Unfortunately, there is no firm prescription for determining the correct amount of smearing to apply to the gauge background. One must find a balance between speeding up convergence of the Dirac operator, reducing chiral symmetry breaking effects, and removing short-distance physics from the gauge field. Of course, when using a fixed number of smearing sweeps n_{sw} , with a constant smearing parameter α , the smearing procedure only introduces irrelevant terms to the action. The fat-link action therefore remains in the same universality class of QCD. Nevertheless, this *freedom*, in the number of smearing sweeps that can be applied to the gauge field, can sometimes be regarded as a drawback to fat-link fermion actions.

The difficulties with implementing exact chiral symmetry on the lattice are summarized by the well known Nielsen-Ninomiya no-go theorem [16]. The no-go theorem forbids the existence of a local lattice Dirac operator, with exact chiral symmetry, and is free of doublers. However, in 1982, Ginsparg and Wilson [17] showed that the physical effects of chiral symmetry will be preserved if one can find a lattice Dirac operator, D , satisfying the Ginsparg-Wilson relation,

$$D\gamma_5 + \gamma_5 D = aDR\gamma_5 D, \quad (2)$$

where R is a local operator. Lüscher later showed [18] that any D , which is a solution of (2), obeys an exact chiral symmetry. A popular solution to the Ginsparg-Wilson relation is the Neuberger Dirac operator [19, 20],

$$D = \frac{m}{a} \left(1 + \frac{D_W(-m)}{\sqrt{D_W^{\dagger}(-m) D_W(-m)}} \right), \quad (3)$$

which satisfies Eq. (2) with $R = 1/m$. Here we consider the standard choice of input kernel, $D_w(-m)$, the Wilson Dirac operator with a negative Wilson-mass term. To produce an acceptable Dirac operator m must lie in the range $0 < m < 2$. For $m < 0$ there are no massless fermions, while for $m > 2$ doublers appear [21]. Varying the choice of m within the allowed range results in a flow of D -eigenvalues, and facilitates a scale-dependent fermionic probe of the gauge field [20].

Any value of m in the range $(0, 2)$ should yield the same continuum behavior [22, 23]. However, simulations are performed at a finite lattice spacing a , and empirical studies prefer $m \gtrsim 0.9$ [24].

The overlap Dirac operator is extremely useful for studies of QCD vacuum structure because it satisfies the Atiyah-Singer index theorem, and will always give an exact integer topological charge. However, the value is not always unique and depends on the value of the Wilson-mass parameter [19, 24, 25, 26]. Studies of the topological susceptibility $\chi = \langle Q^2 \rangle / V$, have also observed this dependence [24, 27]. In particular, the study of Ref. [27] found that χ varied with m for small values of β , but that this dependence decreased as the continuum limit was approached.

In the following, we extend these previous studies to include an analysis of the topological charge density $q(x)$, $Q \equiv \int d^4x q(x)$, as m is varied. In performing an analysis of the topological charge density, rather than χ , we have access to a greater amount of information than that which is learnt from the susceptibility. A change in χ can be due to a change in the mean-square of the topological charge $\langle q^2(x) \rangle$, or to a more fundamental shift in the long-range structure of the vacuum. As such, it is not possible to understand the underlying change in the topological structure from a calculation of χ .

A calculation of the topological charge density is also a useful probe of the gauge field, due to its strong correlation with low-lying modes of the Dirac operator [28, 29], which strongly influence how quarks propagate through the vacuum. Also, while our focus is on the topological charge density, all hadronic observables on the lattice are impacted as we are examining the properties of a lattice fermion action. In recent years, the available compute resources and algorithm enhancements have reached a point where calculations of $q(x)$ using the overlap operator have become feasible [29, 30, 31].

We visualize the topological density as this is currently the most effective way to view the extra information. Our analysis will focus on a comparison between the gluonic topological charge density that is calculated following the application of a smearing algorithm (see Sect. 3). Here our decision is motivated by the growing relevance of fat-link fermion actions. By studying different smearings, we are also able to provide a direct quantitative link to the negative-mass Wilson renormalization parameter of overlap fermions. We gain useful insights into the similarities and differences between these smeared actions and the overlap action, and their relative effectiveness for studies of topological vacuum structure. A central conclusion of this study, is that the ‘‘smoothness’’ of the gauge field, as seen by the overlap operator, depends on the value of the Wilson-mass parameter

2. Simulation details

Due to the high computational effort involved in a full calculation of the overlap topological charge density, we consider a single slice of representative $16^3 \times 32$ lattice configurations. The configurations were generated using a tadpole improved, plaquette plus rectangle (Lüscher-Weisz [32]) gauge action through the pseudo-heat-bath algorithm, with $\beta = 4.80$ giving a lattice spacing of $a = 0.093$ fm.

Five values of the Wilson-mass in the range $(1, 2)$ are used to calculate the overlap topological charge density,

$$q_{ov}(x) = -\text{tr} \left(\gamma_5 \left(1 - \frac{a}{2m} D \right) \right). \quad (4)$$

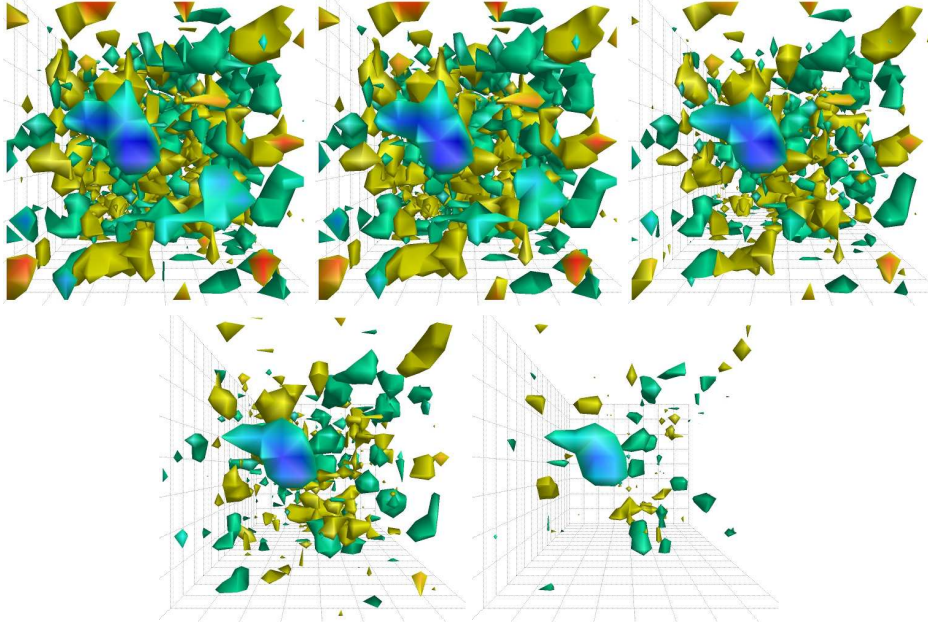


Figure 1: The overlap topological charge density $q_{ov}(x)$ calculated with five choices for the Wilson hopping parameter, κ . Positive regions of topological charge are colored red to yellow, and negative regions are shown as blue to green. From left to right, we have $\kappa = 0.23, 0.21,$ and 0.19 on the first row, with $0.18,$ and 0.17 on the second. There is a clear dependence on the value of κ used, with larger values revealing a greater amount of topological charge density.

Results are reported in terms of the input parameter κ , which at tree level is related to m by

$$\kappa = \frac{1}{2(-m)a + 8r}, \quad (5)$$

with the standard choice $r = 1$. Note that the allowed range for κ is $1/8 < \kappa < 1/4$, and in the interacting theory renormalization leads one to consider $1/6 \lesssim \kappa < 1/4$. A single calculation of $q_{ov}(x)$ for one time-slice will contain $16^2 \times 32 = 8192$ sites of information that must be analyzed, and this most easily achieved through direct visualizations. In all figures, we represent regions of positive topological charge density by the color red fading to yellow, for large to small $q_{ov}(x)$ respectively. Similarly, regions of negative topological charge are colored blue fading to green. A cutoff is applied to the topological charge density, below which no charge is rendered. This allows one to observe the underlying structure of the field.

3. Dependence on the Wilson-mass parameter

The topological charge densities, for the five choices of κ , are presented in Fig. 1. A clear dependence on κ is apparent from the figures, with larger values of κ revealing greater amounts of topological charge. This is consistent with expectations since as κ is increased the Dirac operator becomes more sensitive to smaller topological objects. When using smaller values of κ these objects will not be felt by the Dirac operator.

The removal of nontrivial topological objects as κ is decreased, bears a striking resemblance to the well tested cooling [33, 34, 35, 36, 37, 26] and smearing [38, 39, 40, 41, 42] algorithms. In these procedures, the links on the lattice are systematically updated such that the gauge field is driven towards a more classical state. This results in a removal of topological charge density, as the action is decreased.

The over-improved stout-link smearing algorithm [43] is a modification of the original stout-link algorithm [42]. Instead of the standard single plaquette, a combination of plaquettes and rectangles are used, with the ratio between the two tuned to preserve topology. In every sweep through the lattice, all links are replaced by the smeared links $\tilde{U}_\mu(x)$ [42]

$$\tilde{U}_\mu(x) = \exp(iQ_\mu(x)) U_\mu(x), \quad (6)$$

with

$$Q_\mu(x) = \frac{i}{2}(\Omega_\mu^\dagger(x) - \Omega_\mu(x)) - \frac{i}{6}\text{Tr}(\Omega_\mu^\dagger(x) - \Omega_\mu(x)), \quad (7)$$

and

$$\Omega_\mu(x) = \left(\sum_{\nu \neq \mu} \rho \Sigma_{\mu\nu}^\dagger(x) \right) U_\mu^\dagger(x), \quad (8)$$

where $\Sigma_{\mu\nu}(x)$ denotes the sum of the plaquette and rectangular staples touching $U_\mu(x)$ which reside in the $\mu - \nu$ plane. The ratio of plaquette to rectangular staples is controlled by a new parameter ϵ [43]. In the following we use the suggested value of $\epsilon = -0.25$, which has yielded good results in other studies [29, 44]. For the smearing parameter we select a relatively weak value of $\rho = 0.01$. This should be compared with the maximum value possible for this combination of plaquettes and rectangles, $\rho \approx 0.06$. Whilst in the standard stout-link smearing algorithm, 0.1 is the commonly used value. After smearing, the gluonic topological charge density can be calculated,

$$q_{sm}(x) = \frac{g^2}{32\pi^2} \epsilon_{\mu\nu\rho\sigma} F_{\mu\nu}^{ab}(x) F_{\rho\sigma}^{ba}(x). \quad (9)$$

In order to fairly compare the two definitions for the topological charge density one usually applies a multiplicative renormalization to the gluonic $q_{sm}(x)$ [29],

$$q_{sm}(x) \rightarrow Z q_{sm}(x). \quad (10)$$

This is because after a relatively small amount of smearing the total gluonic topological charge is typically non-integer valued due to the presence of quantum field renormalizations. By matching to the overlap topological charge density we can alleviate this bias.

For this study we have a single slice of the topological charge density and thus can not match the total topological charge. Instead the renormalization factor is chosen such that the *structure* of the two field densities can be best compared. The best match to the overlap $q_{ov}(x)$ is then found by calculating,

$$\min \sum_x (q_{ov}(x) - Z q_{sm}(x))^2, \quad (11)$$

as the number of smearing sweeps is varied. Two methods for calculating Z are considered;

- $Z_{\text{calc}} \equiv \sum_x |q_{ov}(x)| / \sum_x |q_{sm}(x)|$,
- Z_{fit} , where the renormalization factor is calculated such that (11) is minimized.

κ	n_{sw}	Z_{calc}	n_{sw}	Z_{fit}	n_{sw}	Ξ_{AB}
0.17	28	0.56	29	0.47	29	0.76
0.18	26	0.70	27	0.61	27	0.78
0.19	25	0.82	25	0.68	25	0.77
0.21	23	0.91	23	0.76	23	0.75
0.23	22	0.89	23	0.76	23	0.73

Table 1: The number of smearing sweeps, n_{sw} , needed to match the overlap topological charge density calculated with the listed value of κ . The three methods used to find the best match are detailed in the text.

The first definition is motivated by our aim of comparing the structure of the two field densities. The second choice was considered to see if the matching could be improved beyond the first definition. We also compare with an alternative matching procedure [45, 46] in which one calculates,

$$\Xi_{AB} = \frac{\chi_{AB}^2}{\chi_{AA}\chi_{BB}}, \quad (12)$$

with

$$\chi_{AB} = (1/V) \sum_x (q_A(x) - \bar{q}_A)(q_B(x) - \bar{q}_B), \quad (13)$$

where \bar{q} denotes the mean value of $q(x)$, and in our case $q_A(x) \equiv q_{ov}(x)$, $q_B(x) \equiv q_{sm}(x)$. Here the best match is found when Ξ_{AB} is nearest 1. In this case, the ratio eliminates any dependence on the renormalization factor, Z .

We first consider Z_{calc} . The overlap topological charge densities, along with the corresponding best matches, for three choices of κ are shown in Fig. 2. We see that as κ is decreased, and non-trivial topological charge fluctuations are removed, a greater number of smearing sweeps are needed in order to recreate the topological charge density. Again this agrees with expectations since the overlap operator becomes less sensitive to small objects as κ is decreased, and it is these objects that are removed by the smearing algorithm. Comparing the different definitions in Fig. 2 shows good agreement in the topological structures revealed.

The two methods for calculating the renormalization constant Z , together with the values for Ξ , are compared in Table 1. As we move down the table there is a monotonically increasing trend in the number of sweeps required to match the value of κ . We note that despite some minor variation in n_{sw} , it is possible to correlate the number of sweeps to the value of the Wilson hopping parameter. We note that the average renormalization factor $\bar{Z} \sim 0.7$, reflecting the fact that with $\rho = 0.01$ the gauge fields remain rough after ~ 25 sweeps of smearing. The value for Ξ remains approximately constant around ~ 0.75 , suggesting that after renormalizing the level of agreement between the smeared topological charge density and the overlap density is consistent.

4. UV-filtered overlap

Let us now consider the effect of evaluating the overlap operator on a pre-smearing gauge field. This is of some relevance to UV-filtered overlap actions [15, 47, 48, 49], in which all links of a gauge field are smeared prior to applying the overlap operator. As already seen in Fig. 2, applying the overlap operator is in some respects similar to smearing the gauge field. Of interest here is whether the overlap operator, acting on a smeared gauge field, will reveal a topological

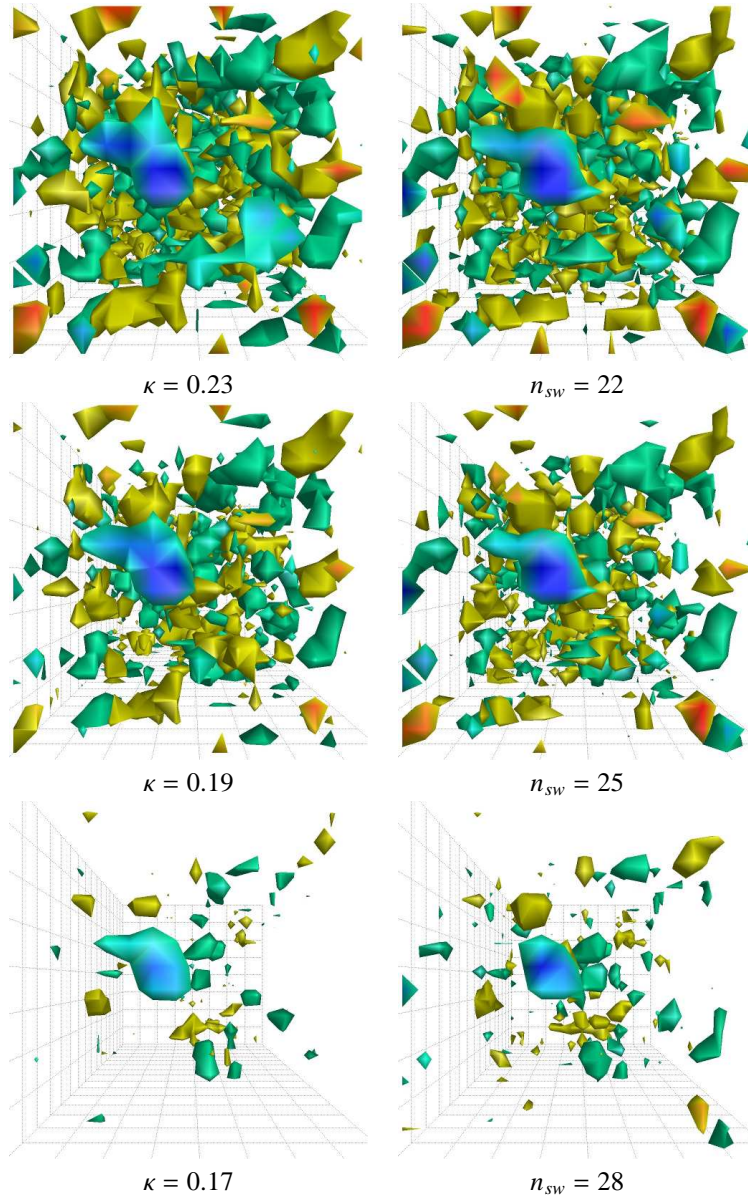


Figure 2: The best smeared matches (right) compared with the overlap topological charge densities (left) in order of decreasing κ , where $q_{sm}(x)$ is renormalised using Z_{calc} . Positive regions of topological charge are colored red to yellow, and negative regions are shown as blue to green. There is a clear relationship between κ and n_{sw} , with smaller κ values requiring a greater number of smearing sweeps to reproduce the topological charge density.

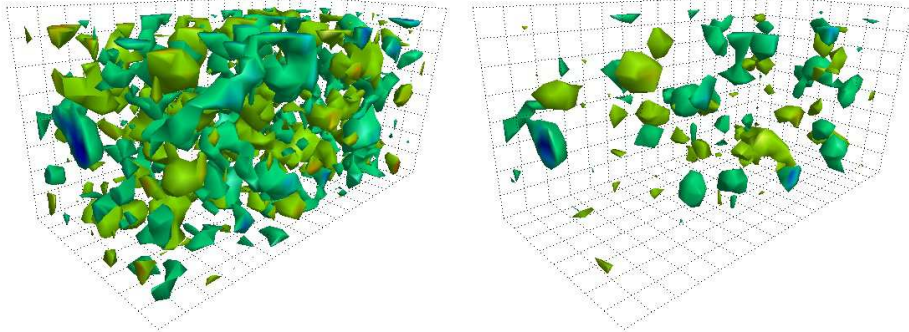


Figure 3: A comparison of the overlap topological charge density $q_{ov}(x)$ computed using $\kappa = 0.19$ (left), with $q_{ov}^{UV}(x)$ calculated using the same κ , on the same configuration, after first applying 25 sweeps of smearing (right). Positive regions of topological charge are colored yellow, and negative regions are shown as blue to green.

charge density close to the input smeared gauge field, or whether further smearing will be needed to match the calculated $q_{ov}(x)$.

To make comparisons clear, we denote the overlap topological charge density, calculated using a smeared configuration as input, by $q_{ov}^{UV}(x)$. We consider the third Wilson-mass, where $\kappa = 0.19$ and the best smeared match was provided by $n_{sw} = 25$. Figure 3 shows the original $q_{ov}(x)$ along with the new UV-filtered $q_{ov}^{UV}(x)$. Far less topological charge density is observed in the pre-filtered case. Given the previous results, it is clear that a far greater number of smearing sweeps will be required to reproduce $q(x)$ using the gluonic definitions.

Repeating the same calculation as before we find that 45 sweeps of over-improved stout-link smearing provides the best match to the overlap topological charge density. A comparison between $q_{ov}^{UV}(x)$ and the smeared $q_{sm}(x)$ is shown in Fig. 4, where $Z_{calc} = 0.85$. This is approximately double the original 25 sweeps required to match the overlap topological charge density, once again revealing the smoothing aspect of the overlap operator. These results indicate that the filtering that occurs in the overlap operator is independent of the input gauge field.

5. Conclusion

Using direct visualizations of the topological charge density, we have analyzed the dependence of the overlap Dirac operator on the Wilson-mass regulator parameter m . As was hinted at by previous studies of the topological susceptibility [24, 27], systematic differences appear in the topological structure of the gauge field as m is varied. By comparing $q_{ov}(x)$ with the gluonic definition of the topological charge density, resolved with a topologically stable smearing algorithm, a direct correlation between m and the number of sweeps is revealed. Smaller values of κ reveal topological charge densities that are similar to using a greater number of smearing sweeps.

From these observations, one can conclude that the “smoothness” of the gauge field, as seen by the overlap operator, depends on the value of the Wilson-mass parameter. This is similar to fat-link fermion actions in which the smoothness is directly dependent upon the number of applied smearing sweeps. These results indicate that the freedom typically associated with fat-

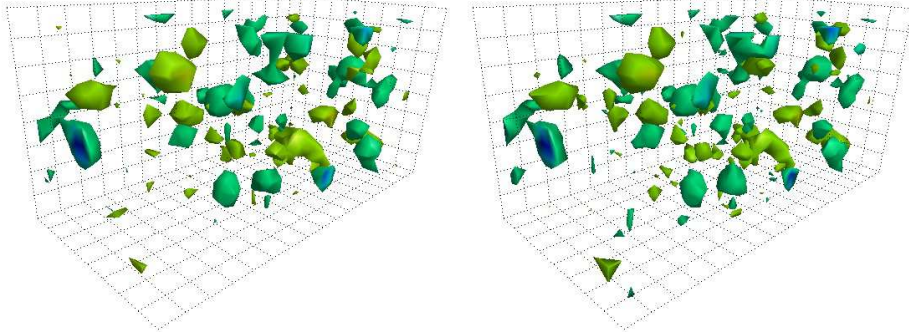


Figure 4: The overlap charge density calculated on a configuration filtered by 25 stout-link smearing sweeps, compared with $q_{sm}(x)$ after 45 sweeps of smearing. Positive regions of topological charge are colored yellow, and negative regions are shown as blue to green. There is a strong correlation between the objects observed. It appears as though the overlap operator has again “smoothed” the configuration.

link fermion actions, through the number of smearing sweeps, is also present in the overlap formalism, through the freedom in the Wilson-mass parameter.

We also considered the application of the overlap operator to a smeared gauge field, which is of relevance to UV-filtered overlap actions. We demonstrated that, regardless of the input gauge field to the overlap operator, UV-filtering still occurs via the overlap operator. The strength of the filtering is of a comparable strength to that of the overlap acting on a hot, unfiltered configuration. When creating a UV-filtered overlap action, one must therefore take care to preserve the short-distance physics of the gauge field.

The topological charge density revealed by the overlap operator is similar to that revealed after 20 to 30 sweeps of stout-link smearing with smearing parameter $\rho = 0.01$, or 2 to 3 sweeps at the standard value of $\rho = 0.1$. In this light, it is important to continue investigations into the extent to which the properties and phenomenology of the overlap operator can be obtained through the use of an efficient Wilson-clover action on smeared configurations.

Future work could also include gauge configurations generated directly using the overlap Dirac operator, or possibly with an alternate overlap definition based on staggered fermions [50], which may prove more computationally efficient than the usual Wilson-based overlap operator.

Acknowledgments

This research was undertaken on the NCI National Facility in Canberra, Australia, which is supported by the Australian Commonwealth Government. We also acknowledge eResearch SA for generous grants of supercomputing time which have enabled this project. This research is supported by the Australian Research Council. J. B. Zhang is partly supported by Chinese NSFC-Grant No. 10675101 and 10835002.

References

- [1] Kenneth G. Wilson. Confinement of quarks. *Phys. Rev.*, D10:2445–2459, 1974.

- [2] B. Sheikholeslami and R. Wohlert. Improved continuum limit lattice action for qcd with wilson fermions. *Nucl. Phys.*, B259:572, 1985.
- [3] S. Durr et al. Ab-initio determination of light hadron masses. *Science*, 322:1224–1227, 2008.
- [4] Thomas A. DeGrand, Anna Hasenfratz, and Tamas G. Kovacs. Optimizing the chiral properties of lattice fermion actions. 1998.
- [5] Thomas A. DeGrand, Anna Hasenfratz, and Tamas G. Kovacs. Instantons and exceptional configurations with the clover action. *Nucl. Phys.*, B547:259–280, 1999.
- [6] Anna Hasenfratz, Roland Hoffmann, and Stefan Schaefer. Hypercubic smeared links for dynamical fermions. *JHEP*, 05:029, 2007.
- [7] Stefano Capitani, Stephan Durr, and Christian Hoelbling. Rationale for uv-filtered clover fermions. *JHEP*, 11:028, 2006.
- [8] S. Durr et al. Scaling study of dynamical smeared-link clover fermions. *Phys. Rev.*, D79:014501, 2009.
- [9] James M. Zanotti et al. Hadron masses from novel fat-link fermion actions. *Phys. Rev.*, D65:074507, 2002.
- [10] J. M. Zanotti, B. Lasscock, D. B. Leinweber, and A. G. Williams. Scaling of flic fermions. *Phys. Rev.*, D71:034510, 2005.
- [11] Sharada Boinepalli, Waseem Kamleh, Derek B. Leinweber, Anthony G. Williams, and James M. Zanotti. Improved chiral properties of flic fermions. *Phys. Lett.*, B616:196–202, 2005.
- [12] Waseem Kamleh, Ben Lasscock, Derek Bruce Leinweber, and Anthony Gordon Williams. Scaling analysis of flic fermion actions. *Phys. Rev.*, D77:014507, 2008.
- [13] N. Cundy et al. Non-perturbative improvement of stout-smeared three flavour clover fermions. *Phys. Rev.*, D79:094507, 2009.
- [14] Thomas A. DeGrand, Anna Hasenfratz, and Tamas G. Kovacs. Improving the chiral properties of lattice fermions. *Phys. Rev.*, D67:054501, 2003.
- [15] Waseem Kamleh, David H. Adams, Derek B. Leinweber, and Anthony G. Williams. Accelerated overlap fermions. *Phys. Rev.*, D66:014501, 2002.
- [16] Holger Bech Nielsen and M. Ninomiya. No go theorem for regularizing chiral fermions. *Phys. Lett.*, B105:219, 1981.
- [17] Paul H. Ginsparg and Kenneth G. Wilson. A remnant of chiral symmetry on the lattice. *Phys. Rev.*, D25:2649, 1982.
- [18] Martin Luscher. Exact chiral symmetry on the lattice and the ginsparg-wilson relation. *Phys. Lett.*, B428:342–345, 1998.
- [19] Rajamani Narayanan and Herbert Neuberger. A construction of lattice chiral gauge theories. *Nucl. Phys.*, B443:305–385, 1995.
- [20] Herbert Neuberger. Exactly massless quarks on the lattice. *Phys. Lett.*, B417:141–144, 1998.
- [21] Ferenc Niedermayer. Exact chiral symmetry, topological charge and related topics. *Nucl. Phys. Proc. Suppl.*, 73:105–119, 1999.
- [22] David H. Adams. Axial anomaly and topological charge in lattice gauge theory with overlap-Dirac operator. *Annals Phys.*, 296:131–151, 2002.
- [23] David H. Adams. On the continuum limit of fermionic topological charge in lattice gauge theory. *J. Math. Phys.*, 42:5522–5533, 2001.
- [24] Robert G. Edwards, Urs M. Heller, and Rajamani Narayanan. Spectral flow, chiral condensate and topology in lattice qcd. *Nucl. Phys.*, B535:403–422, 1998.
- [25] Rajamani Narayanan and Pavlos M. Vranas. A numerical test of the continuum index theorem on the lattice. *Nucl. Phys.*, B506:373–386, 1997.
- [26] J. B. Zhang et al. Numerical study of lattice index theorem using improved cooling and overlap fermions. *Phys. Rev.*, D65:074510, 2002.
- [27] Luigi Del Debbio and Claudio Pica. Topological susceptibility from the overlap. *JHEP*, 02:003, 2004.
- [28] Daniel-Jens Kusterer, John Hedditch, Waseem Kamleh, Derek B. Leinweber, and Anthony G. Williams. Low-lying eigenmodes of the wilson-dirac operator and correlations with topological objects. *Nucl. Phys.*, B628:253–269, 2002.
- [29] E. M. Ilgenfritz et al. Vacuum structure revealed by over-improved stout-link smearing compared with the overlap analysis for quenched qcd. *Phys. Rev.*, D77:074502, 2008.
- [30] I. Horvath et al. On the local structure of topological charge fluctuations in qcd. *Phys. Rev.*, D67:011501, 2003.
- [31] E. M. Ilgenfritz et al. Exploring the structure of the quenched qcd vacuum with overlap fermions. *Phys. Rev.*, D76:034506, 2007.
- [32] M. Luscher and P. Weisz. On-shell improved lattice gauge theories. *Commun. Math. Phys.*, 97:59, 1985.
- [33] B. Berg. Dislocations and topological background in the lattice o(3) sigma model. *Phys. Lett.*, B104:475, 1981.
- [34] M. Teper. Instantons in the quantized su(2) vacuum: A lattice monte carlo investigation. *Phys. Lett.*, B162:357, 1985.

- [35] Ernst-Michael Ilgenfritz, M. L. Laursen, G. Schierholz, M. Muller-Preussker, and H. Schiller. First evidence for the existence of instantons in the quantized $su(2)$ lattice vacuum. *Nucl. Phys.*, B268:693, 1986.
- [36] Sundance O. Bilson-Thompson, Derek B. Leinweber, and Anthony G. Williams. Highly-improved lattice field-strength tensor. *Ann. Phys.*, 304:1–21, 2003.
- [37] S. O. Bilson-Thompson, D. B. Leinweber, A. G. Williams, and G. V. Dunne. Comparison of $|Q| = 1$ and $|Q| = 2$ gauge-field configurations on the lattice four-torus. *Annals Phys.*, 311:267–287, 2004.
- [38] M. Falcioni, M. L. Paciello, G. Parisi, and B. Taglienti. Again on $su(3)$ glueball mass. *Nucl. Phys.*, B251:624–632, 1985.
- [39] M. Albanese et al. Glueball masses and string tension in lattice qcd. *Phys. Lett.*, B192:163–169, 1987.
- [40] Frederic D. R. Bonnet, Derek B. Leinweber, Anthony G. Williams, and James M. Zanotti. Improved smoothing algorithms for lattice gauge theory. *Phys. Rev.*, D65:114510, 2002.
- [41] Anna Hasenfratz and Francesco Knechtli. Flavor symmetry and the static potential with hypercubic blocking. *Phys. Rev.*, D64:034504, 2001.
- [42] Colin Morningstar and Mike J. Peardon. Analytic smearing of $su(3)$ link variables in lattice qcd. *Phys. Rev.*, D69:054501, 2004.
- [43] Peter J. Moran and Derek B. Leinweber. Over-improved stout-link smearing. *Phys. Rev.*, D77:094501, 2008.
- [44] Peter J. Moran and Derek B. Leinweber. Impact of dynamical fermions on qcd vacuum structure. *Phys. Rev.*, D78:054506, 2008.
- [45] Falk Bruckmann et al. Quantitative comparison of filtering methods in lattice qcd. *Eur. Phys. J.*, A33:333–338, 2007.
- [46] F. Bruckmann et al. Comparison of filtering methods in $su(3)$ lattice gauge theory. *PoS, CONFINEMENT8*:045, 2008.
- [47] Wolfgang Bietenholz. Convergence rate and locality of improved overlap fermions. *Nucl. Phys.*, B644:223–247, 2002.
- [48] Tamas G. Kovacs. Locality and topology with fat link overlap actions. *Phys. Rev.*, D67:094501, 2003.
- [49] Stephan Durr, Christian Hoelbling, and Urs Wenger. Physics prospects of uv-filtered overlap quarks. *Nucl. Phys. Proc. Suppl.*, 153:82–89, 2006.
- [50] David H. Adams. Theoretical foundation for the Index Theorem on the lattice with staggered fermions. *Phys. Rev. Lett.*, 104:141602, 2010.